JACS
JOURNAL OF THE AMERICAN CHEMICAL SOCIETY
Article
pubs.acs.org/JACS

Dye-Sensitized Photocathodes: Efficient Light-Stimulated Hole Injection into p-GaP Under Depletion Conditions

Michelle Chitambar,[†,¶] Zhijie Wang,[‡,¶] Yiming Liu,[§] Angus Rockett,[⊥] and Stephen Maldonado*[,†,‡]

[†]Applied Physics Program, University of Michigan, 450 Church Street, Ann Arbor, Michigan 48109, United States
[‡]Chemistry Department, University of Michigan, 930 North University, Ann Arbor, Michigan 48109, United States
[§]Institute of Photoelectronic Thin Film Device and Technology, Nankai University, Weijin Road 94, Tianjin 300071, PR China
[⊥]Materials Science and Engineering, University of Illinois, 1304 West Green Street, Urbana, Illinois 61801, United States

Supporting Information

ABSTRACT: The steady-state photoelectrochemical responses of p-GaP photoelectrodes immersed in aqueous electrolytes and sensitized separately by six triphenylmethane dyes (rose bengal, rhodamine B, crystal violet, ethyl violet, fast green fcf, and brilliant green) have been analyzed. Impedance measurements indicated that these p-GaP(100) photoelectrodes operated under depletion conditions with an electric field of ~8.5×10^5 V cm^{-1} at the p-GaP/solution interface. The set of collected wavelength-dependent quantum yield responses were consistent with sensitization occurring specifically from adsorbed triphenylmethane dyes. At high concentrations of dissolved dye, the measured steady-state photocurrent−potential responses collected at sub-bandgap wavelengths suggested unexpectedly high (>0.1) net internal quantum yields for sensitized hole injection. Separate measurements performed with rose bengal adsorbed on p-GaP surfaces pretreated with $(NH_4)_2S$ verified efficient sensitized hole injection. A modified version of wxAMPS, a finite-difference software package, was utilized to assess key operational features of the sensitized p-GaP photocathodes. The net analysis showed that the high internal quantum yield values inferred from the experimental data were most likely afforded by the internal electric field present within p-GaP, effectively sweeping injected holes away from the interface and minimizing their participation in deleterious pathways that could limit the net collection yield. These simulations defined effective threshold values for the charge carrier mobilities ($\geq 10^{-6}$ cm^2 V^{-1} s^{-1} and $\geq 10^{-1}$ cm^2 V^{-1} s^{-1} at dopant densities of 10^{18} and 10^{13} cm^{-3}, respectively), hole injection rate constants ($\geq 10^{12}$ s^{-1}), and surface trap densities (10^{12} cm^{-2}) needed to attain efficient hole collection with the quality of p-GaP materials used here. The cumulative experimental and modeling data thus provide insight on design strategies for assembling new types of dye-sensitized photocathodes that operate under depletion conditions.

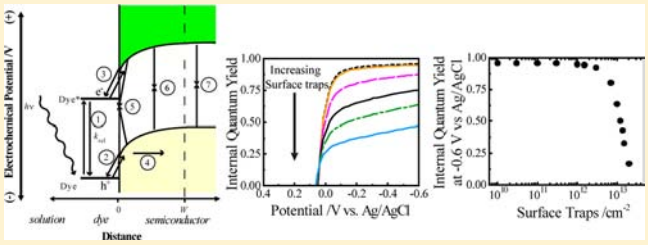

INTRODUCTION

As the only commercially available photoelectrochemical cell for solar energy conversion, n-type metal oxide nanoparticle films coated with adsorbed molecular chromophores have largely defined dye-sensitized photoelectrochemistry for the past two decades.[1−3] Specifically, the current dogma for the design of dye-sensitized photoelectrochemical cells consists of five nearly immutable features: (1) wide-bandgap metal oxides, (2) panchromatic dyes that overcome the minimal sunlight absorbance by metal oxides such as TiO_2, (3) charge injection of photoexcited *electrons* from an excited chromophore into an n-type semiconductor immersed in a nonaqueous solution (Figure 1a), (4) sunlight to electricity *conversion*, and (5) ultrasmall semiconductor nanoparticles that provide a large surface area for dye loading but are too small to support appreciable internal electric fields.[4]

An alternative direction in dye-sensitized photoelectrochemistry is the development of dye-sensitized photocathodes. Several reports have recently detailed sensitized p-type nanoparticle film photocathodes for solar-to-electrical energy conversion.[5−18] Many of these efforts use dye-sensitized photocathodes as a means to supplement/boost the activity of conventional dye-sensitized photoanodes. Alternatively, comparatively few efforts have focused on understanding and exploiting sensitized *hole* injection processes in their own right. This report describes specifically the operation of dye-sensitized p-type phosphide photoelectrodes in aqueous electrolytes (Figure 1b). Such photocathodes are interesting for both fundamental and practical reasons. First, the valence band energetics of phosphides favor sensitized hole injection as compared to the valence band energetics of most metal oxides[19,20] (Figure 1b), facilitating measurement of sensitized hole injection from a variety of dyes. Second, sensitized photocathodes in water are naturally suited for solar to chemical *storage* since the regeneration of the reduced dye

Received: April 26, 2012
Published: June 18, 2012

 © 2012 American Chemical Society dx.doi.org/10.1021/ja304019n | J. Am. Chem. Soc. 2012, 134, 10670−10681

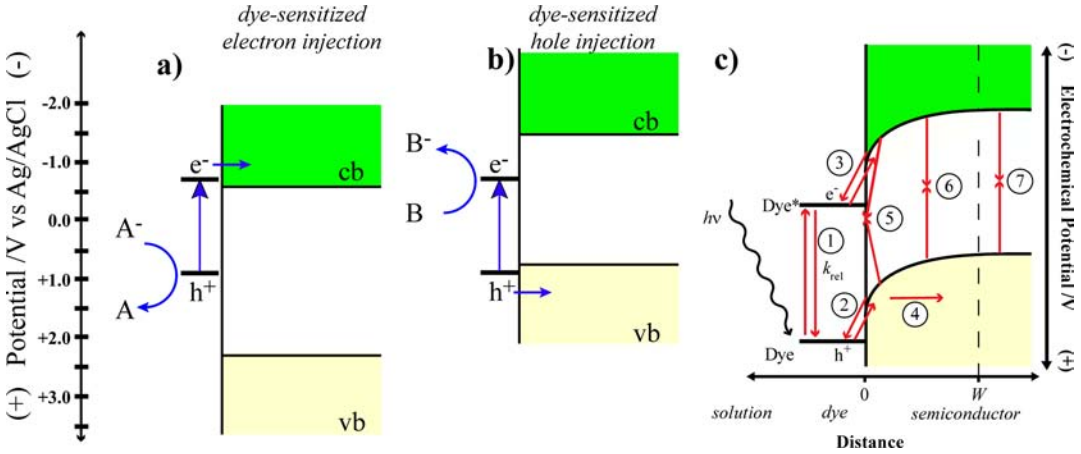

Figure 1. Depiction of dye sensitization at semiconductor photoelectrodes. (a) Dye-sensitized electron injection from a photoexcited chromophore at the surface of a metal oxide semiconductor. (b) Dye-sensitized hole injection from a photoexcited chromophore at the surface of a phosphide semiconductor. (c) Dye-sensitized hole injection from a photoexcited chromophore at the surface of a phosphide semiconductor under depletion conditions. The constituent processes that favor and limit the magnitude of the net sensitized photocurrent are enumerated. These processes are (1) optical excitation/relaxation of the dye, (2) hole transfer between the dye and semiconductor, (3) electron transfer between the dye and semiconductor, (4) electric-field-induced transport within the semiconductor, (5) charge recombination at surface states at the semiconductor interface, (6) charge recombination in the depletion region, and (7) charge recombination in the bulk of the semiconductor.

(following hole injection) can be coupled with reductive transformations in solution (Figure 1b). The development of such sensitized photocathodes requires a thorough understanding of all rate-impacting processes.

Our initial efforts in this area are focused on sensitized gallium phosphide (GaP) photoelectrodes,[21] which have several properties advantageous for study. First, GaP can be prepared/obtained with well-defined bulk optoelectronic properties (e.g., mobility and dopant density) that are favorable for efficient light-harvesting systems. Second, as will be described in detail herein, dye-sensitized p-GaP can support substantial levels of light-stimulated hole injection. In contrast to previous reports of dye-sensitized p-CuSCN,[14,17] p-NiO,[6,8,9,11,13,18,22] and p-CuO,[16] this report details high internal quantum yields attainable with p-GaP photoelectrodes specifically operating under depletion conditions (i.e., featuring a large internal electric field). Third, the response characteristics of planar p-GaP photoelectrodes operating under depletion conditions can be readily modeled and understood using finite-difference simulations, offering the opportunity for detailed analysis.[23] Fourth, as a midsized bandgap semiconductor, GaP can absorb light at wavelengths shorter than 550 nm, relaxing the required panchromaticity of a sensitizer for complete absorbance of sunlight.

We present data for single-crystalline p-GaP(100) photoelectrodes operated under potentiostatic control and sensitized by a set of triphenylmethane dyes in aqueous solution. Specifically, data are presented for two xanthene dyes (rose bengal (RB) and rhodamine B (Rh B)), two triaminotriphenylmethane dyes (crystal violet (CV) and ethyl violet (EV)), and two diaminotriphenylmethane dyes (fast green fcf (FG) and brilliant green (BG)). We report and assess the observed steady-state photoelectrochemical responses with these dyes, highlighting the unusually high internal quantum yields (>0.1) observed at p-GaP photoelectrodes without prior optimization in the form of surface passivation or dye engineering. Through comparison of experimental results to those generated from a finite-difference model, we conclude that the promising photoelectrochemical responses for these dye-sensitized systems are due to the presence of an internal electric field within the depletion layer at the p-GaP photoelectrode surface. A version of the Analysis of Microelectronic and Photonic Structures (AMPS) code previously used to study solid-state photovoltaics[24,25] was modified specifically for this work. The experimental system investigated herein was modeled with wxAMPS[16,25] to identify explicitly how experimentally controllable features such as surface trap density, charge transfer rate, and the bulk optoelectronic properties of the semiconductor photoelectrode impacted the attainable net quantum yields for sensitized charge injection at steady state. Finally, aspects relevant to designing efficient phosphide-based dye-sensitized cells are discussed.

EXPERIMENTAL SECTION

Chemicals and Materials. Rhodamine B (95%), ethyl violet (≥80%), crystal violet (≥90%), fast green (≥85%), rose bengal (95%), brilliant green (98%), copper phthalocyanine-3,4′,4″,4‴-tetrasulfonic acid tetrasodium salt (85%), nickel(II) phthalocyanine tetrasulfonic acid tetrasodium salt (50%), methyl viologen dichloride (98%), ammonium sulfide (20%, aqueous solution), and potassium chloride (≥99%) were used as received from Sigma Aldrich. Concentrated HCl(aq) and 40% v/v NH_4F(aq) were obtained from Fisher Scientific and Transene, respectively. Zinc(II) phthalocyanine tetrasulfonic acid was obtained and used as received from Frontier Scientific. H_2O was purified (>18 MΩ cm) with a Barnstead Nanopure III purifier and used throughout. N_2(g) and O_2(g) were obtained from Metro Welding. GaP photoelectrodes were prepared from a 400 μm thick, single-crystalline, single-side polished p-type GaP(100) wafer doped with Zn at 1.1×10^{18} cm^{-3} and featured a hole mobility of 70 cm^2 V^{-1} s^{-1}. GaP wafers were obtained and used as received from ITME.

Electrodes and Photoelectrochemical Cell. GaP wafers were diced into 0.5 cm × 0.5 cm sections and ohmic contacts were prepared by etching the back side for 30 s with concentrated NH_4F, rinsing with distilled H_2O, soldering a thin, even film of an In−Zn amalgam onto the etched surface, and annealing for 10 min at 400°C. Electrodes were then prepared by using silver print (GC Electronics) to attach the GaP section to a copper wire coil threaded through a glass tube and sealing with inert epoxy (Hysol C). Unless otherwise indicated, electrodes were etched for 30 s in 12.1 M HCl(aq), rinsed with H_2O, dried under N_2(g) and immediately used. Photoelectrochemical measurements were made in an airtight quartz cell with an optically flat bottom. A

dx.doi.org/10.1021/ja304019n | J. Am. Chem. Soc. 2012, 134, 10670−10681

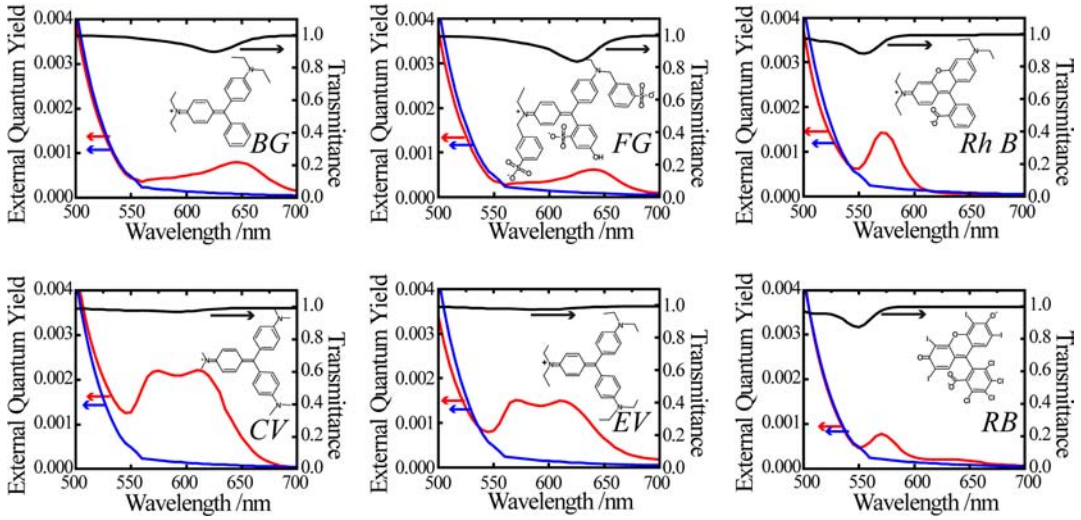

Figure 2. Measured wavelength dependence for net photocurrent generation of p-GaP(100) electrodes poised at −0.6 V vs Ag/AgCl while immersed either in (blue) only deaerated 1 M KCl(aq) or (red) deaerated 1 M KCl(aq) containing 5 μM dissolved dye; *BG* = brilliant green, *FG* = fast green fcf, *Rh B* = rhodamine B, *CV* = crystal violet, *EV* = ethyl violet, *RB* = rose bengal. The transmitted light through the ∼1 mm spacing between the electrode face and optical window is indicated in black (right-hand *y*-axes). The structure of each dye (without counterions) is also shown.

carbon fiber counter electrode and a Ag/AgCl reference electrode were used. For all photoelectrochemical measurements, the distance between the optical window and GaP photoelectrode face was nominally 1 mm. One molar KCl was used as the background electrolyte unless noted otherwise. For measurements with adsorbed rose bengal, p-GaP(100) electrodes were first etched, rinsed, dried, and then soaked in ammonium sulfide solution for 6 h. The pH of the ammonium sulfide solution was set to 7 through addition of HCl(aq) aliquots.[26] This treatment resulted in surface-bound ammonium moieties. Electrodes were then immersed in aqueous solutions containing rose bengal for 30 min followed by an immersion in nanopure water for 1 h to remove weakly physisorbed dye before undergoing further photoelectrochemical analyses.

Optical and Photoelectrochemical Measurements. All measurements were performed at room temperature (23 ± 3 °C). Transmittance measurements were obtained with a Varian Cary 5000 ultraviolet−visible−near-infrared (UV−Vis−NIR) photospectrometer. Absorptance (i.e., the fraction of total light absorbed) values are reported rather than absorption values, where noted. All photoelectrochemical measurements were performed in a three-electrode cell under potentiostatic control (Princeton Applied Research 267A), facilitating analysis of the specific operation of the dye-sensitized photocathode. The net photocurrent collected per incident light intensity is reported here as an external quantum yield on a scale from 0 to 1. Internal quantum yield, also given on a scale from 0 to 1, represents the net photocurrent collected per absorbed light intensity. Wavelength-dependent external quantum yield measurements were taken with a setup described previously.[27] Illumination intensities ranged from ∼0.1 to 1.0 mW cm^{-2}. External quantum yield measurements were corrected for solution transmittance using the Beer−Lambert relation and dye absorption spectra as measured with a Cary 5000 UV−Vis−NIR photospectrometer. Internal quantum yield values were calculated by dividing the measured external quantum yield values by the fraction of incident light absorbed by a monolayer of dye. Monolayer absorptance was estimated via the Beer−Lambert relation, with the extinction coefficient determined from transmittance measurements of dilute dye solutions. The density of an idealized close-packed dye monolayer was estimated using the areal footprint of the dye oriented parallel to the surface plane. Current−potential characteristics were measured either under monochromatic illumination from a 150 W Xe arc lamp and an Oriel quarter-turn single-grating monochromator (both Newport) or with a 500 mW green LED laser. The latter source type was used specifically for intensity dependence measurements.

Steady-State Model of Dye-Sensitized Charge Injection. The net efficiency for charge injection between a photoexcited dye and a p-type semiconductor under depletion conditions (Figure 1c) is controlled primarily by features intrinsic to the semiconductor (hole mobility, internal electric field, band energetics, charge carrier lifetimes and populations), the dye (excited state lifetime, ground and excited state redox potentials), and the interface (rate of heterogeneous charge transfer). To determine the explicit dependence and interplay of the features described in Figure 2 on net sensitized charge injection at steady state, a custom-designed variant of AMPS (wxAMPS) was used. wxAMPS is a software package for modeling planar semiconductor heterojunctions in one dimension that utilizes the finite-difference method to determine the concentration of charge carriers throughout the system as a function of position and applied potential according to eqs 1 and 2,

$$-\frac{\delta}{\delta x}\left(\epsilon(x)\frac{\delta\phi(x)}{\delta x}\right) = q\rho \tag{1}$$

$$\frac{\delta J_n}{\delta x} = -qG(x) + qR(x) \tag{2a}$$

$$\frac{\delta J_p}{\delta x} = qG(x) - qR(x) \tag{2b}$$

where ϕ is the local electric potential, q is the unsigned charge of an electron, ϵ is the material dielectric constant, ρ is the summed (free, ionized impurity, and trapped) charge density, J_n is the electron current density, J_p is the hole current density, $G(x)$ is the optical generation rate of carriers at x, and $R(x)$ is the total charge carrier recombination rate at x. Equation 1 is Poisson's equation, relating charge carrier populations and the electric potential in one dimension.[23] Equations 2a and 2b are the current continuity equations for electrons and holes, respectively.[23] The key revision made to the version of AMPS used in this work is a reformulation of the boundary conditions at the material interfaces. Charge transfer rates between GaP and a dye layer were expressed in the general framework used for semiconductor electrochemistry and the principle of detailed balance.[28,29] Equations 3a and 3b describe the electron and hole current densities at the interface between the adsorbed dye and GaP,

dx.doi.org/10.1021/ja304019n | J. Am. Chem. Soc. 2012, 134, 10670−10681

$$-J_n = qk^0_{et}\, e^{\frac{-((E_{LUMO,Dye}-E_{cb,GaP})-\lambda)^2}{4k_BT\lambda}} N_{cb,GaP}[dye]_0 \left(\frac{[dye^*]}{[dye]_0} - \frac{n_{s,GaP}}{n_{s0,GaP}}\right) \quad (3a)$$

$$J_p = qk^0_{ht}\, e^{\frac{-((E_{vb,GaP}-E_{HOMO,Dye})+\lambda)^2}{4k_BT\lambda}} N_{vb,GaP}[dye]_0 \left(\frac{[dye^*]}{[dye]_0} - \frac{p_{s,GaP}}{p_{s0,GaP}}\right) \quad (3b)$$

where each term is defined in Table 1. The origin of these boundary conditions is discussed in detail in section S2 in the Supporting Information (SI). Notably, in eq 3 the electron and hole charge transfer rate constants (k^0_{et} and k^0_{ht}, respectively) and concentrations refer to adsorbed dyes. Although the basic design of this version of AMPS allows for the input of heterogeneous rate constants with the more familiar units of $cm^4\ s^{-1}$ for charge transfer to an acceptor in solution,[28] the model used herein has been designed so that this rate constant translates directly to that of an *adsorbed* dye with units of $cm^3\ s^{-1}$ through division of the input rate constant by the dye layer thickness. The products of these modified rate constants and the effective densities of states ($k^0_{ht} \times N_{vb,GaP}$ and $k^0_{et} \times N_{cb,GaP}$, respectively) have units of s^{-1} and are commensurate with the charge injection rates from an adsorbed dye. Accordingly, direct comparison to published reports of experimentally measured charge injection rates from spectroscopic quenching measurements can be made. Monolayers of adsorbed dye were approximated by defining a 5 Å dielectric layer at the GaP surface with the optical, electrical, and electrochemical properties appropriate for a generic organic dye (SI). A description of all the default input parameters, including mesh size, spacing used for discretization, and recombination velocities at the front and back contacts, is given in section S3 in the SI.

Table 1. List of Terms

symbol	description	symbol	description
q	unsigned charge of electron	$E_{cb,GaP}$	GaP conduction band edge
k_B	Boltzmann's constant	$E_{vb,GaP}$	GaP valence band edge
T	temperature	$N_{cb,GaP}$	effective density of states in GaP conduction band
$E_{LUMO,Dye}$	LUMO energy for dye	$N_{vb,GaP}$	effective density of states in GaP valence band
$E_{HOMO,Dye}$	HOMO energy for dye	$n_{s,GaP}$	GaP surface electron concentration
λ	charge transfer reorganization energy	$p_{s,GaP}$	GaP surface hole concentration
$[dye]_0$	surface concentration of dye in the dark at equilibrium	$n_{s0,GaP}$	GaP surface electron concentration in the dark at equilibrium
$[dye^*]$	surface concentration of photoexcited dye at steady-state under illumination	$p_{s0,GaP}$	GaP surface hole concentration in the dark at equilibrium

RESULTS

Sensitization of p-GaP with Dyes Dissolved in Aqueous Solutions. In deaerated 1 M KCl, impedance measurements with freshly etched p-GaP electrodes yielded an apparent flatband potential of +0.98 ± 0.16 V vs Ag/AgCl (SI, Figure S2), indicating an approximate value for the potential of the valence band edge, $E_{vb,GaP}$, of +1.02 ± 0.19 V vs Ag/AgCl. Since the open circuit rest potential of these electrodes was typically ~0 V vs Ag/AgCl, these p-GaP electrodes were under strong depletion conditions and supported internal electric field strengths, ξ, of $\sim 8.5 \times 10^5$ V cm^{-1}.[30] The flatband potential, barrier height, and GaP valence band level inferred from capacitive measurements changed by several tenths of a volt for electrodes that were allowed to age in solution for prolonged periods of time. Accordingly, all subsequent measurements were performed immediately after immersion into the test solution.

Figure 2 illustrates the observed photoelectrochemical responses for p-GaP(100) photoelectrodes biased at −0.6 V vs Ag/AgCl while immersed in deaerated 1 M KCl(aq) containing various organic sensitizers at a concentration of 5 μM. Each dye solution elicited a photocurrent response with a wavelength dependence that followed the absorptance profile of each respective dye. The peak molar extinction coefficients from 500 to 700 nm for these dyes ranged between 10^7 to 10^8 mol^{-1} cm^2. For each presented dye solution, measurable photocurrent was obtained at sub-bandgap wavelengths, i.e. at wavelengths corresponding to energies smaller than the bandgap energy of 2.26 eV (549 nm) for GaP. Under the employed conditions, the magnitudes of the external quantum yields for all six dyes at this concentration ranged from 0.001 to 0.002. Replacing the p-GaP photoelectrodes with a metal electrode in these electrolytes did not produce any detectable net photocurrents. The total light transmitted through the dye solution is indicated in black in Figure 2. Correction of the experimentally measured external quantum yields for optical losses incurred by light absorption from the dye solution through the ~1 mm path length between the cell window and electrode surface did not substantially change the profiles shown in Figure 2 (SI, Figure S3). Hence, at 5 μM, the observed photoelectrochemical responses qualitatively indicated the innate spectral profile for sensitization by each dye. Notably, for each plot in Figure 2, the wavelength corresponding to the maximum sub-bandgap external quantum yield was uniformly offset from the wavelength of maximum absorbance of the dissolved dye (Table 2), consistent with the notion that sensitization occurred specifically through *adsorbed* dye at the photoelectrode surface.[14,31−34] Sensitized photocurrents at sub-bandgap wavelengths were not observed for all investigated dyes. Specifically, sensitization was not detected in electrolytes containing dissolved metal phthalocyanine tetrasulfonic acid dyes (SI, Figure S4) with standard potentials for oxidation that were more negative than $E_{vb,GaP}$.[35]

Table 2. Dye Absorptance and Sensitization Properties

	dye	absorptance peak[a] /nm	sensitization peak[b] /nm
BG	brilliant green	625	645
FG	fast green fcf	624	640
Rh B	rhodamine B	555	570
CV	crystal violet	590	610
EV	ethyl violet	595	610
RB	rose bengal	549	570

[a]Measured at 7.5 μM in water. [b]Maximum quantum yield at sub-bandgap wavelengths measured at 5 μM in 0.1 M KCl(aq) with p-GaP poised at E = −0.6 V vs Ag/AgCl.

For every dye shown in Figure 2, the measured sensitized photocurrents were a function of the concentration of dissolved dye in solution. Figure 3 shows a representative plot highlighting the observed dependence of the external quantum yield of rhodamine B at 570 nm (i.e., wavelength of maximum sensitization) on the dissolved concentration of rhodamine B. At low (<50 μM) concentrations, the sensitized photocurrent

dx.doi.org/10.1021/ja304019n | J. Am. Chem. Soc. 2012, 134, 10670−10681

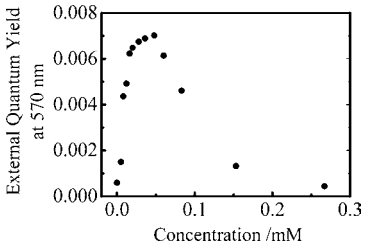

Figure 3. Observed dependence of the as-measured external quantum yields for a p-GaP(100) electrode recorded at 570 nm as a function of the concentration of rhodamine B. The electrode was poised at −0.6 V vs Ag/AgCl and immersed in a 1 M KCl(aq) electrolyte containing dissolved dye.

markedly increased with increasing concentration of rhodamine B, consistent with the premise that higher adsorbed dye concentrations were promoted by higher solution concentrations. At approximately 50 μM, the measured photocurrents reached a maximum value and then decreased with further increase in concentration. At the highest concentrations, the total light loss by absorption of dye dissolved in bulk solution was significant (transmittance ≤0.4). Optical correction of the transmittance losses at the highest concentrations was difficult due to the strong dependence on the absolute distance between the cell window and p-GaP surface and is not incorporated in Figure 3. Hence, for every dye listed in Figure 2, additional photoelectrochemical responses for p-GaP(100) photoelectrodes biased at −0.6 V vs Ag/AgCl while immersed in deaerated 1 M KCl(aq) with dye concentrations of 50 μM were collected (SI, Figure S5). Each dye elicited a sub-bandgap photoresponse that qualitatively followed those shown in Figure 2, except convoluted more strongly with light absorption from the bulk solution. This effect contributed to slight shifts in the wavelengths corresponding to the maximum photocurrents.

The photocurrent−potential profiles for p-GaP(100) electrodes in these dye solutions are presented in Figure 4. Each plot represents typical photoresponses obtained with monochromatic illumination (nominal power density of 0.3 mW cm^{-2}) at the wavelength corresponding to the maximum photocurrent response in 50 μM dye solution. The dashed line at the top of each plot serves as a reference value that corresponds to the expected quantum yield from a close-packed monolayer of adsorbed dye that injects photogenerated holes with an internal quantum yield of 1, accounting for light transmission losses through the bulk solution (SI, Figure S6). For each plot in Figure 4, two photoelectrochemical responses are shown that illustrate the behaviors observed in aerated and deaerated solutions, respectively. Several features were uniformly observed for all six dyes. First, all measured responses yielded external quantum yield values at −0.6 V vs Ag/AgCl that were at least 10% of the predicted value for a close-packed monolayer operating with an internal quantum yield of 1. These features implied that the *internal* quantum yields for sensitized hole injection in all of these systems were ≥0.1. Second, sensitized photocurrents measured in aerated solutions were uniformly larger at every potential than sensitized photocurrents measured in deaerated solutions. The degree of difference between photocurrent−potential responses recorded in aerated and deaerated solutions varied across all six dyes but seemed consistent within each subset of xanthene, triaminotriphenylmethane, and diaminotriphenylmethane dyes. No photoelectrochemical response recorded in aerated solutions exceeded the expected limit for a close-packed monolayer operating with an internal quantum yield of 1, although the responses for the triaminotriphenylmethane dyes (crystal violet and ethyl violet) implied internal quantum yields >0.5. Third, the profiles of the photoelectrochemical responses recorded in aerated solutions were more rectangular, i.e. attained the plateau photocurrent value at potential closer to the rest potential. For the triaminotriphenylmethane dyes, the

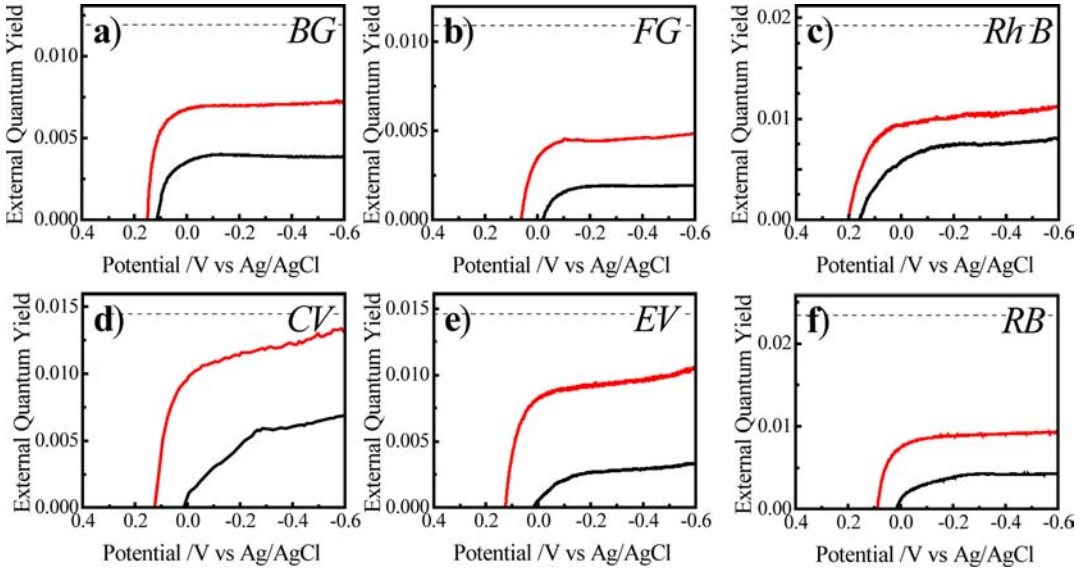

Figure 4. Measured potential dependence for net photocurrent generation of p-GaP(100) electrodes under monochromatic illumination while immersed in aerated or deaerated 1 M KCl(aq) containing 50 μM dissolved dye; *BG* = brilliant green, *FG* = fast green fcf, *Rh B* = rhodamine B, *CV* = crystal violet, *EV* = ethyl violet, *RB* = rose bengal. Red and black lines indicate measurements obtained in electrolytes that were sparged with O_2(g) and N_2(g), respectively. Each measurement was done at a wavelength that corresponded to the maximum external quantum yield in Figure 2. The dashed line near the top indicates the response for an ideal monolayer coverage of each dye operating with an internal quantum yield of 1 (i.e., every absorbed photon yields a carrier that is collected as current).

dx.doi.org/10.1021/ja304019n | J. Am. Chem. Soc. 2012, 134, 10670−10681

photoresponses did not reach a true plateau photocurrent value within the potential range of interest.

The effect of a dissolved redox mediator on measured photoresponses was further investigated by replacing O_2 with the outer-sphere redox couple methyl viologen ($MV^{2+/+}$) at a concentration of 10^{-2} M. The addition of $MV^{2+/+}$ increased both the attainable photocurrents and open-circuit rest potentials under illumination for all dyes relative to responses measured in deaerated solutions without a dissolved mediator. However, these responses were uniformly lower than the responses in aerated solutions. Still, the augmented photoresponses in the presence of O_2 were inconsistent with hole injection from sensitized singlet oxygen, $O_2(^1\Delta)$, rather than from the photoexcited dye. First, all of the investigated triphenylmethane dyes yielded comparable sensitization levels even though the capacity of each triphenylmethane dye to generate $O_2(^1\Delta)$ varies considerably. Specifically, although the xanthene triarylmethane dyes are efficient sensitizers for $O_2(^1\Delta)$ generation,[36,37] the two triaminotriphenylmethane dye types are known to not produce $O_2(^1\Delta)$ readily under illumination.[38,39] Second, photoelectrochemical measurements with ethyl violet were performed before, during, and after injection of a large excess of $O_2(^1\Delta)$ quenchers (SI, Figure S8). N_3^- and histidine are strong 'physical' and 'chemical' quenchers, respectively, of $O_2(^1\Delta)$ in solution. Appreciable suppression of the sensitized photocurrent measured with ethyl violet was not observed after addition of either 2 mM N_3^- or 2 mM histidine. Third, no photocurrents were observed with illumination at sub-bandgap wavelengths in experiments that employed Zn(II) phthalocyanine tetrasulfonic acid as the sensitizer (SI, Figure S4). Zn(II) phthalocyanine tetrasulfonate has previously been shown as an efficient sensitizer for generation of $O_2(^1\Delta)$ under illumination in aqueous solution.[40] Fourth, the peak wavelengths for sensitization were red-shifted relative to the absorbance band of each dye dissolved in solution, consistent with the premise that dye specifically at the p-GaP interface was the primary sensitizing species rather than $O_2(^1\Delta)$ generated in bulk solution.

Sensitization of p-GaP by an Adsorbed Dye. The six dyes featured in Figures 2 and 4 did not possess functional groups suitable for deliberate binding to etched GaP(100) surfaces. Accordingly, emersion of p-GaP(100) photoelectrodes from the dye solutions used in Figure 4 did not produce consistent dye loadings that persisted after reimmersion in 1 M KCl(aq). However, prior treatment of p-GaP(100) surfaces with $(NH_4)_2S$(aq) did facilitate the persistent adsorption of rose bengal. Following treatment with $(NH_4)_2S$(aq), immersion of GaP(100) surfaces in aqueous solutions with 6 mM rose bengal for 30 min resulted in an appreciable amount of adsorbed dye. Figure S7 (SI) highlights the absorptance at sub-bandgap wavelengths measured for a GaP(100) substrate treated in this way. Figure 5a shows the wavelength-dependent external quantum yield responses recorded for p-GaP(100) photoelectrodes that were first treated with $(NH_4)_2S$(aq), soaked in aqueous solutions of rose bengal with varied concentrations for 30 min and then transferred to a deaerated solution of 1 M KCl(aq). The magnitude of the photoresponse at wavelengths >550 nm strongly followed the concentration of dye in solution during the soaking (adsorptive) step, increasing after being soaked in more concentrated solutions. Figure 5b shows a plot of the measured external quantum yield at 570 nm as a function of the concentration of rose bengal during the soaking (adsorptive) step. The line in Figure 5b is a fit of the

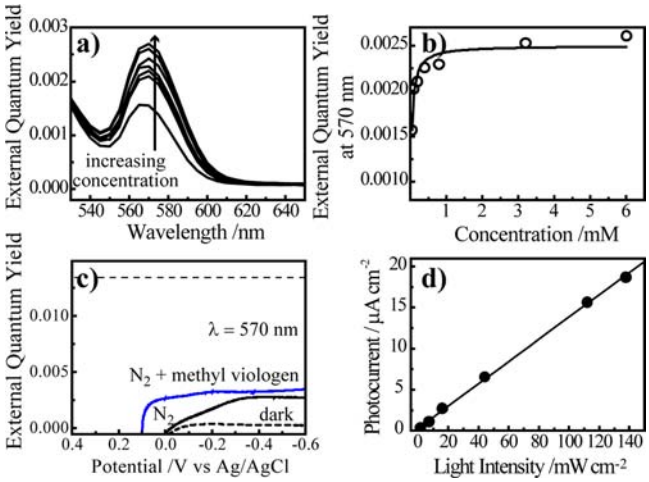

Figure 5. (a) Measured external quantum yield at sub-bandgap wavelengths for a p-GaP(100) photoelectrode immersed in deaerated 1 M KCl(aq). The electrode was previously treated with $(NH_4)_2S$(aq) as described in the text and soaked in aqueous solutions containing concentrations of dissolved rose bengal ranging from 0.05 mM to 6 mM for 30 min. (b) Dependence of the measured external quantum yield at 570 nm as a function of the concentration of rose bengal in the solution used for dye adsorption. The line indicates a fit to a Langmuir adsorption model with an adsorption constant of 2.8×10^4 M^{-1}. (c) Measured potential dependence of p-GaP(100) sensitized with adsorbed rose bengal via a 30 min soak in a 6 mM solution while (black dashed line) in the dark or (solid lines) illuminated with 570 nm light at 0.34 mW cm^{-2}. The black solid line indicates observed response in deaerated solution with no methyl viologen dichloride. The blue solid line shows the measured response after addition of 10 mM methyl viologen dichloride. The black dashed line indicates the expected photocurrent if sensitization occurred with unity internal quantum yield for the given loading of adsorbed dye. (d) Measured dependence of the photocurrent obtained with a p-GaP(100) electrode sensitized by adsorbed rose bengal on monochromatic light intensity.

data to a simple Langmuir adsorption model with a binding constant of 2.8×10^4 M^{-1}. Figure 5c highlights representative photoelectrochemical responses obtained with monochromatic illumination at 570 nm and a p-GaP(100) electrode in deaerated 1 M KCl that was first soaked in 6 mM rose bengal solution for 30 min. In the absence of illumination, p-GaP(100) electrodes showed no appreciable cathodic currents in the investigated potential range. Photoresponses obtained under illumination in deaerated solutions featured a decidedly nonrectangular photocurrent−potential profile. The plateau photocurrent at −0.6 V vs Ag/AgCl, in conjunction with the measured absorptance of the adsorbed rose bengal in Figure S7 (SI), corresponded to an internal quantum yield of 0.17. Photoresponses obtained under illumination in deaerated solutions with 10 mM methyl viologen yielded a modestly higher plateau photocurrent value at −0.6 V vs Ag/AgCl. However, the addition of methyl viologen dichloride more significantly changed two other aspects of the overall photocurrent−potential profiles. First, the rest potential under illumination was shifted approximately +0.1 V. Second, the photocurrent−potential profile was significantly more 'rectangular', i.e. the plateau photocurrent was obtained at potentials closer to the open-circuit rest potential. P-type GaP(100) photoelectrodes with deliberately adsorbed rose bengal in solutions containing methyl viologen all showed good response characteristics at higher photon fluxes. Figure 5d shows that the

dx.doi.org/10.1021/ja304019n | J. Am. Chem. Soc. 2012, 134, 10670−10681

plateau photocurrent at −0.6 V vs Ag/AgCl was linearly dependent on the illumination intensity from 1.6 to 140 mW cm^{-2}.

Finite-Difference Modeling of the Steady-State Photoresponses of Sensitized p-GaP. Modeling studies were performed to isolate the contributions from specific carrier transport processes to the observed steady-state photoelectrochemical responses of sensitized p-GaP(100). Specifically, these simulations were employed to interpret the unexpectedly high internal quantum yields observed in this work and to determine quantitatively the interplay between the processes identified in Figure 1. Accordingly, simulations were performed using system parameters that approximated the experimental conditions present in this work (SI, section S3). The simulation results in Figures 6−8 describe the sensitized photoresponse of a p-GaP photoelectrode under the same depletion conditions as for the data in Figures 2, 4, and 5. Since this modeling approach was one-dimensional, all simulations corresponded to a perfect monolayer of dye at the p-GaP surface. The simulation results in Figures 6−8 model the responses of a sensitized p-GaP photoelectrode illuminated with 625 nm light at 0.3 mW cm^{-2} as a function of changes in several system variables. In these plots, the ratio of the net collected carrier flux and the total light flux absorbed by the dye film represents the internal quantum yield of the sensitized system.

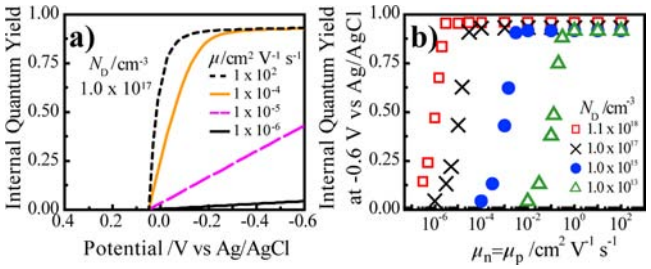

Figure 6. (a) Modeling results for the potential dependence of the internal quantum yield for sensitized hole injection as a function of charge carrier mobility within p-GaP at $N_D = 1.0 \times 10^{17}$ cm^{-3}. (b) The internal quantum yield for hole injection modeled at −0.6 V vs Ag/AgCl as a function of charge carrier mobility at four different dopant densities: 1.1×10^{18} cm^{-3} (red open squares), 1.0×10^{17} cm^{-3} (black ×'s), 1.0×10^{15} cm^{-3} (blue filled circles) and 1.0×10^{13} cm^{-3} (green open triangles). Major simulation parameters: $k_{inj} = 3.8 \times 10^{14}$ s^{-1}; $N_t = 5 \times 10^{10}$ cm^{-2}.

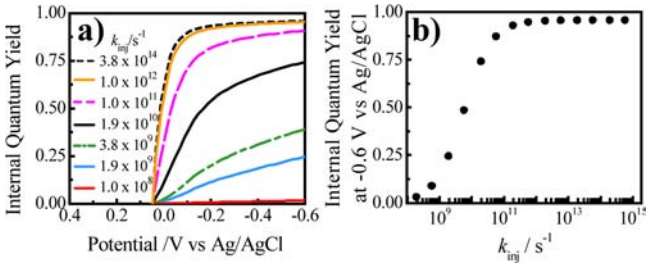

Figure 7. (a) Modeling results for the potential dependence of the internal quantum yield for sensitized hole injection for various values of the interfacial charge transfer rate, k_{ht}, for GaP electrodes with $N_t = 10^{10}$ cm^{-2}. (b) The internal quantum yield for hole injection at −0.6 V vs Ag/AgCl as a function of k_{ht}. Major simulation parameters: $N_D = 1.1 \times 10^{18}$ cm^{-3}; $\mu_n = \mu_p = 100$ cm^2 V^{-1} s^{-1}; $N_t = 5 \times 10^{10}$ cm^{-2}.

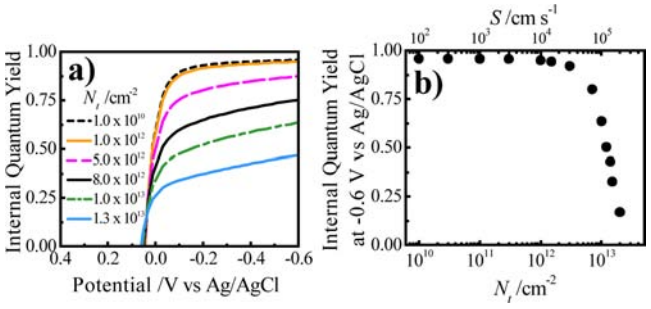

Figure 8. (a) Modeling results for the potential dependence of the internal quantum yield for sensitized hole injection at various GaP surface trap densities. (b) The modeled internal quantum yield for hole injection at −0.6 V vs Ag/AgCl as a function of surface trap density. The corresponding values for surface recombination velocity are also shown. Major simulation parameters: $N_D = 1.1 \times 10^{18}$ cm^{-3}; $\mu_n = \mu_p = 100$ cm^2 V^{-1} s^{-1}; $k_{inj} = 3.8 \times 10^{14}$ s^{-1}.

Figure 6 shows a set of simulation results that specifically describe the influence of process (4) in Figure 1c, i.e. the drift-based removal of majority carriers from the interface following charge injection, with the parameters for the other processes held constant. Figure 6a shows the dependence of the internal quantum yield on applied potential for values of charge carrier mobility, μ, spanning 8 orders of magnitude in p-GaP with doping density $N_D = 10^{17}$ cm^{-3}. At this doping density, simulation results indicated that μ values $\geq 10^{-4}$ cm^2 V^{-1} s^{-1} were sufficient to sustain the maximum net photocurrent at an applied bias of −0.6 V vs Ag/AgCl. Charge carrier mobility values less than 10^{-4} cm^2 V^{-1} s^{-1} resulted in a steep drop in overall energy conversion at this value of N_D, effected both by decreased photocurrents and a loss of rectangularity in the photocurrent−potential profile. Figure 6b summarizes these data for several values of N_D. For $N_D = 10^{17}$ cm^{-3}, the internal quantum yield at −0.6 V vs Ag/AgCl dropped precipitously to zero at a mobility value of 10^{-6} cm^2 V^{-1} s^{-1}. Simulations with other dopant density values show similar behavior, with the falloff in high vs low internal quantum yield occurring at larger charge carrier mobility values for lower values of N_D. For a dopant density of 1.1×10^{18} cm^{-3}, the simulations indicated a threshold charge carrier mobility value of 10^{-6} cm^2 V^{-1} s^{-1}. For a dopant density of 1.0×10^{13} cm^{-3}, charge carrier mobilities $\geq 10^{0}$ cm^2 V^{-1} s^{-1} were required to obtain high net internal quantum yields. In total, the data in Figure 6 indicated that the doping level (1.1×10^{18} cm^{-3}) and mobility properties (70 cm^2 V^{-1} s^{-1}) of the p-GaP(100) materials used in this work were sufficient to afford high internal quantum yields.

Figure 7 presents a series of simulations that detail the effect of changes in process (2) in Figure 1, i.e. the heterogeneous charge transfer of holes between the adsorbed dye and the p-GaP valence band, with the parameters for the other relevant processes held constant. Figure 7a shows a set of photocurrent−potential responses that feature values of k_{inj} that span 5 orders of magnitude. For simulations with hole transfer occurring at frequencies faster than 10^{12} s^{-1}, the model predicted high internal quantum yields for sensitization and rectangular photocurrent−potential profiles. For simulations with hole transfer frequencies slower than 10^{12} s^{-1}, the model indicated pronounced changes in the photoelectrochemical response. Although the rest potential under illumination was not predicted to change appreciably, the attainable photocurrent at −0.6 V vs Ag/AgCl and sharpness of the

dx.doi.org/10.1021/ja304019n | J. Am. Chem. Soc. 2012, 134, 10670−10681

photocurrent−potential profile decreased gradually as the time scales for hole transfer increased. Figure 7b shows that the model predicted a drop of the internal quantum yield to ∼0 when k_{inj} was 10^8 s^{-1}. Conversely, these simulations indicated a minimum value of 10^{12} s^{-1} for k_{inj} to ensure that process 2 in Figure 1 was not the rate-limiting factor in the sensitization process.

Figure 8 shows a series of simulations that illustrate the effect of changes to process (5) in Figure 1, i.e. Shockley−Read−Hall charge recombination at surface states at the semiconductor/dye interface. In Figure 8a, the photocurrent−potential responses are shown at several values of the surface trap density, N_t. For Shockley−Read−Hall recombination, N_t is proportional to the total surface recombination velocity, S, through eq 4,

$$S = \sigma v_T N_t \quad (4)$$

where σ is the effective surface trap cross section ($\sim 10^{-15}$ cm^{-2}) and v_T is the thermal velocity (10^7 cm s^{-1}) of carriers in GaP. N_t values from 10^{10} to 10^{14} cm^{-2} for these simulations corresponded to S values between 10^2 and 10^6 cm s^{-1}. Assuming a nominal surface atom density of 10^{15} cm^{-2}, this range of N_t values corresponded to surfaces with as few as one trap per 100,000 surface atoms and as many as one trap per 10 surface atoms. The results in Figure 8a show no appreciable change in the sensitized photocurrent−potential response for N_t values between 10^{10} and 10^{12} cm^{-2} ($10^2 \leq S \leq 10^4$ cm s^{-1}), implying that surface recombination is not rate limiting for defect densities on the order of one trap per 1000+ surface atoms. For higher surface trap densities, the photocurrent−potential profile became slightly less square and did not plateau at more negative potentials. The principal effect, however, was a strong attenuation of the maximum attainable photocurrent density. Figure 8b details this point more explicitly. The internal quantum yield at −0.6 V vs Ag/AgCl estimated from these simulations dropped sharply for $N_t > 2 \times 10^{12}$ cm^{-2}. The model results indicated attainable quantum yields of <0.1 for defect densities greater than one trap per 100 surface atoms ($N_t > 10^{13}$ cm^{-2}).

DISCUSSION

The major conclusions from the data shown here are that sensitized hole injection from a variety of common triphenylmethane dyes to p-GaP immersed in an aqueous electrolyte has been confirmed and that p-GaP photoelectrodes under depletion conditions supported sensitization with high internal quantum yields in otherwise nonoptimized systems. These data collectively provide insight on new strategies for designing high-efficiency sensitized photoelectrodes. These points are discussed in detail below.

Sensitized Hole Injection in Water. Several results from the photoelectrochemical measurements in 1 M KCl(aq) performed with sensitizers either dissolved in solution or adsorbed onto p-GaP implicate sensitized hole injection from adsorbed excited chromophores into the valence band of GaP. First, in both measurement types, the general spectral profile of the measured cathodic external quantum yields followed the absorptance profile of each dissolved dye, indicating sub-bandgap photocurrents arose specifically due to the photoexcited dye. In all cases, the wavelength for maximum absorptance was red-shifted from the wavelength of maximum sensitization. Irrespective of whether the dye was purposely tethered to the electrode surface or partitioned from solution onto the electrode surface (i.e., physisorbed), a red-shift in the sensitized spectrum is a hallmark of sensitized injection from photoexcited chromophores specifically at a semiconductor electrode interface[14,32−34] and suggests that a sensitization process occurred at the semiconductor electrode/electrolyte interface. Second, sensitized cathodic currents were only measured in experiments featuring dyes with excited states that had enough oxidizing strength to abstract an electron from (i.e., inject a hole into) p-GaP(100). Specifically, the triphenylmethane dyes have standard potentials for oxidation equal to or more positive than $E_{vb,GaP}$.[41−44] In contrast, assuming redox properties similar to that of Zn phthalocyanine, the first oxidation process for Zn phthalocyanine tetrasulfonate is at a significantly more negative potential[35] (∼+0.76 V vs SCE) than for this set of triphenylmethane dyes. Accordingly, these observations are consistent with the general sensitization scheme described in Figure 1 and further indicate that the cathodic photocurrents do not arise purely from reduction of photogenerated species dissolved in solution. In addition, the observed photoelectrochemical responses were inconsistent specifically with the reduction of $O_2(^1\Delta)$ generated from photoexcited dye. Notably, hole injection from $O_2(^1\Delta)$ (generated via energy transfer from a dissolved photoexcited chromophore) into p-type semiconductors in acetonitrile has been noted previously. Specifically, Grätzel and Frei reported photoreduction of $O_2(^1\Delta)$ in acetonitrile with dissolved methylene blue after irradiation with visible light and raised the possibility that the main overall source of cathodic photocurrent at sub-bandgap wavelengths in other systems was hole injection from photogenerated singlet oxygen, $O_2(^1\Delta)$.[45] However, the observed invariance of cathodic photocurrents measured here in the presence of known, potent $O_2(^1\Delta)$ quenchers and the lack of sensitized photocurrents specifically in experiments containing Zn phthalocyanine tetrasulfonate directly counter this premise. A similar increase in hole injection levels in the presence of O_2 has been reported for cyanine dyes adsorbed onto CuSCN and was attributed to O_2 accepting electrons from depleted chromophores.[14] Although the specific sensitivity of the observed sensitized photoresponses toward dissolved, reducible species in solution like MV^{2+} and O_2 was not elucidated here, these cumulative observables strongly support the notion that sensitized hole injection from photoexcited triphenylmethane dyes at the p-GaP(100) surface was the primary process responsible for the measured photocurrent.

Influence of an Internal Electric Field on the Net Photocurrent Yield. A notable finding from this report is the measurement of uniformly high (>0.1) internal quantum yields for hole injection from all investigated triphenylmethane dyes into p-GaP(100) in aqueous electrolytes. These systems possessed several features that could preclude efficient charge injection. First, the dyes were not bonded to the surface of GaP through well-defined covalent bonds. Even for purposely adsorbed rose bengal using GaP surfaces pretreated with $(NH_4)_2S$, there was no deliberate attempt to strongly couple the dye and p-GaP electronically. Second, all measurements were performed in an aqueous electrolyte where suppressed sensitization levels are common.[46] Third, no measures were taken to preserve the electronic integrity of p-GaP(100) surfaces. As is common with most III−V semiconductors, the native oxide on p-GaP that forms quickly in ambient conditions is known to have an exorbitantly high density of surface traps ($N_t \geq 10^5$ cm^{-2}).[47,48] The cumulative effect of these three

separate aspects could be expected to severely limit the measurable level of sensitized photocurrents. Clearly, the results shown here indicate that a separate feature(s) mitigated these three possible problems.

The combined experimental and modeling results implicate the internal electric field within the p-GaP(100) photoelectrodes in this study as a primary factor for why high internal quantum yields were observed. As observed here, freshly etched, nondegenerately doped p-GaP(100) in this electrolyte in the dark possesses nominally a 1 V potential drop in the near-surface region. The resultant electric field within the near-surface region of GaP will direct any holes at the interface away from the surface toward the bulk (Figure 1c) at a drift velocity, v_d,

$$v_d = \mu_p \xi \tag{5}$$

The results shown here specifically suggest that large values of v_d in sensitized photoelectrodes are sufficient to offset suboptimal conditions such as poor (ill-defined) dye connectivity to the surface and a high density of surface trap states. To be clear, these data do not suggest that sensitized photoelectrodes cannot operate with high efficiency for charge injection in the absence of an appreciable internal electric field. The prevalence and success of the system popularized by O'Regan and Grätzel clearly show that high net charge injection yields are possible at semiconductor photoelectrodes with little or no internal electric fields. However, one interpretation of the present work is that the inability to support large internal electric fields limits the possible means to achieve maximum energy conversion. In the conventional sensitized photoanodes described by O'Regan and Grätzel, a high net collection efficiency was obtained only with a specific set of semiconductor, dye, and redox couple components that collectively featured fortuitously slow deleterious chemical/electrochemical rates.[49,50] In essence, that system leveraged only chemical/molecular aspects to achieve high net collection efficiencies. Enormous efforts over the past two decades have been directed at modifying one or many of the chemical components, with little overall gains or improvement.[4] In fact, only recently have sensitized systems with substantially different dyes, semiconductor morphologies, and redox couples been able to attain high efficiencies.[51−59]

As described in Figure 1c, a sensitized photoelectrode that possesses a large internal electric field (i.e., operates under depletion conditions) can also utilize rapid carrier drift to suppress deleterious processes. Specifically, a sufficiently large value of v_d limits the availability of holes at the photoelectrode interface to participate in deleterious chemical/electrochemical processes. The successful competition of carrier drift processes with undesirable electrochemical reactions at semiconductor photoelectrodes under strong depletion conditions underpins the field of nonsensitized regenerative photoelectrochemistry.[60] Sweeping majority carriers away from semiconductor electrode interfaces through carrier drift in the depletion region has been exploited to produce nonsensitized semiconductor/liquid heterojunctions with solar energy conversion properties that match or exceed conventional solid state semiconductor photovoltaics.[61] In the context of dye-sensitized systems, the value and utility of internal electric fields has been less clearly defined.

Recently, a modeling report concluded that internal electric fields within nanostructured TiO_2 photoelectrodes would not substantially augment their performance as sensitized photoanodes in the standard cell design.[62] The findings reported here do not contradict that work. Instead, the modeling results and the apparent high internal quantum yields measured experimentally in this work indicate that carrier drift within a semiconductor electrode can ameliorate the operation of sensitized systems in systems with 'suboptimal' rates for relevant *chemical* processes. Several other groups have postulated this beneficial feature of sensitized semiconductor electrodes operating under depletion conditions. Most notably, Spitler et al. utilized a model based on an Onsager treatment to describe the influence of electric fields in the depletion region on carrier transport.[63,64] Separately, Parkinson et al.[65] and Honda et al.[66,67] have independently reported data that show low sensitized photocurrents at either undoped or lightly doped planar semiconductor photoelectrodes that cannot support large internal electric fields. The modeling performed with the wxAMPS code in this work directly describes this phenomenon and indicates that high net sensitization yields are achievable when the semiconductor electrode supports an appreciable electric field and charge carrier mobilities are above a threshold value, consistent with both our current results and previous reports.

Numerous modeling approaches have been used to describe the operation of dye-sensitized cells.[68−75] The majority of these models were not designed to describe a semiconductor photoelectrode under depletion conditions, and many do not provide direct chemical insight into the kinetic properties of the system. The salient feature of the wxAMPS code used in this work is that rather than using an approach based on an equivalent circuit modeling[70,71,73] or one that assumes transport conditions,[68,69,72,76] a direct, quantitative description of the interrelation of several system parameters is possible for a planar photoelectrode sensitized by a dye layer. The approach taken here with wxAMPS could be further improved to address submonolayer dye loadings, image charges,[63] and possible Frumkin corrections[77] for heterogeneous rate constants. The latter point has been previously shown to be small for semiconductor electrodes under depletion conditions as compared to metal electrodes, where the primary potential drop is across the double layer in solution and can sometimes affect the rate of charge transfer by more than an order of magnitude.[77] Irrespective, the interpretation of the data shown here is that, if bulk optoelectronic properties such as dopant density and charge carrier mobility are sufficiently large to minimize deleterious 'back' charge transfer processes (Figure 1c), efficient sensitization does not require ultrafast (10^{-15} s) time scales for hole transfer and/or semiconductor surfaces that are rigorously free of surface trap states ($<10^{10}$ cm^{-2}) to function. Instead, semiconductor photoelectrodes operating under strong depletion conditions should have a high tolerance toward both slow interfacial charge transfer rates with an adsorbed chromophore and high populations of trap states. More detailed studies are needed to further describe the generality of these 'tolerances.' Nevertheless, these simulation results are in line with the empirical observations for sensitized p-GaP(100).

Design Strategies for Achieving Large External Quantum Yields from Sensitized Photocathodes in Water. The data shown here for planar, macro-scale p-GaP electrodes provide useful insight on design criteria for sensitized photocathodes with high external quantum yields and, correspondingly, the capacity for efficient solar energy conversion/storage. One obvious requisite feature is a higher

total optical absorptance by the sensitizer film. A planar photoelectrode coated by a sensitizer monolayer with an absorption coefficient of 10^8 mol^{-1} cm^2 can have an absorptance value of ~0.01, representing the upper limit for the external net quantum yield for charge injection if the internal net quantum yield is 1. For lightly doped semiconductors with poor electronic properties in 'nonoptimized' cells (e.g., no I_3^-/I^-, *tert*-butyl pyridine, N3 dye, etc.), low internal quantum yields require a significant (>1000) increase in total surface area to support enough dye to achieve high external quantum yields.[4] In contrast, for a sensitized semiconductor under depletion conditions operating with an internal quantum yield of 1, electrodes with an order of magnitude smaller surface area would likewise achieve high external quantum efficiency. A p-GaP electrode that has just 2 orders of magnitude greater surface area than that of a planar electrode is still capable of supporting large internal electric fields[78] and could in principle support high external quantum yields. Ultrasmall semiconductor nanoparticles (<50 nm) provide ample surface areas but cannot typically support large internal electric fields.[78] However, alternative photoelectrode form factors with high aspect ratios can satisfy both criteria. Although sensitized nanowires/nanotubes in the conventional dye-sensitized photoanode design have been explored,[79−81] sensitized high aspect ratio p-GaP photoelectrodes have yet to be explored in the context of the work presented here. Previously, we have demonstrated that doped thin nanowire arrays[82] and macroporous films[27] with large aspect ratios (>10^2) that support appreciable internal electric fields can function as promising photoelectrodes for conversion of supra-bandgap illumination with high quantum yields. An additional advantage of high aspect ratio GaP architectures is their excellent light-scattering properties at sub-bandgap wavelengths,[83] an aspect that could be used to further increase the effective light absorptance of a sensitizer coating without sacrificing the ability to operate under depletion conditions.

A second feature required in sensitized photocathodes with high external quantum yields for hole injection is a different/improved surface chemistry relative to the native surface of p-GaP(100). Three separate deficiencies in the surface chemistry of GaP must be addressed. First, the native interface of GaP is prone to chemical attack and degradation.[84] Second, the native surface of GaP has a high density of electronic defects.[47,48] Third, the typical binding mode strategies for dyes on metal oxides like TiO_2 are not appropriate for the native surface of GaP. Unlike for indium phosphide (InP),[85] neither native nor thermal oxides are tenable surfaces for GaP in optoelectronic applications. Recent results from our group suggest a possible wet chemical surface modification strategy to circumvent these issues. Deliberate alkylation of GaP interfaces using nucleophilic (Grignard) reagents has been shown to be a viable strategy for introducing organic groups that substantially impede chemical degradation of the surfaces of GaP and related III−V materials.[86] Further, the same alkylation chemistry has been shown to lower substantially trap densities at GaAs interfaces.[87] Additional work is needed to determine to what extent surface traps can be reduced at GaP surfaces. However, the simulation results in this work suggest that only a modest decrease in surface trap density to a level of 10^{12} traps cm^{-2} (approximately 1 trap per 1000 surface atoms) would effect a meaningful gain in the internal quantum yield. This benchmark is significant because significantly lower densities of surface traps are presently unattainable for most semiconductor materials but are not necessary for this application under depletion conditions equivalent to those shown here. Further work is also needed to demonstrate whether functional groups that simultaneously passivate electronic defects (i.e., do not involve binding through surface oxides) as well as introduce secondary chemical handles for binding sensitizers are possible. The attachment scheme used here with ammonium sulfide provided a means to make measurements with persistently adsorbed sensitizer. However, none of the data presented here featured a dye attached to p-GaP(100) through a well-defined, stable covalent bond. In all cases, each dye was randomly physisorbed. A binding strategy that uses deliberate chemical bonding has more potential for long-term stability. The experimental data shown here for persistently adsorbed rose bengal and the simulation results for k_{inj} demonstrate that sensitization can occur without deliberately induced strong electronic coupling, potentially widening the useful bonding motifs that can be used to tether a sensitizer to the electrode surface.

A final comment can be made regarding two additional aspects in the design of sensitized photocathodes. Many of the desirable features identified here (band edge energetics, capacity to be doped p-type, large charge carrier mobilities) are not specific to GaP. P-type InP has long been recognized as a potential photocathode material in water.[88,89] However, many other binary and ternary phosphides with the same or related crystal structures (zincblende and chalcopyrite, respectively) also share many of these desirable properties without including rare earth elements such as In.[90] Related phosphides like BP and $ZnGeP_2$ have been prepared with high aspect ratio form factors.[91,92] Separately, this work did not focus on identifying particular dye-redox mediator combinations. Sensitizer/redox mediator combinations that can be used for a fuel-forming reaction such as $H^+(aq)$ reduction to H_2 would enable such sensitized photocathodes to be used for generating chemical fuels rather than solely electricity. A recent report that describes dissolved H_2 generation in water by cobalt complexes sensitized with rhodamine B suggests such systems may be possible.[93]

■ CONCLUSION

The cumulative experimental and modeling results shown here illustrate an alternative design strategy for constructing dye-sensitized photoelectrochemical systems that differ in composition, configuration, and function from existing convention in the arena of dye-sensitized solar cells. Specifically, the present report shows that sensitized hole injection from photoexcited dyes is readily observed at p-type GaP photoelectrodes. Further, when operating under depletion conditions, p-GaP photoelectrodes support sensitization with high internal quantum yields in aqueous electrolytes. Electrochemical measurements and finite-difference simulations using a modified version of the wxAMPS program showed that these high internal quantum yield values were most likely afforded by the internal electric fields present in the depletion region in GaP. These fields effectively swept injected holes away from the interface and minimized their participation in deleterious pathways that would otherwise limit their net collection yield. The results of these simulations defined effective benchmark values in dopant density, charge carrier mobilities, injection rate constants, and surface trap densities for attaining high net internal quantum yields for hole collection. Operating dye-sensitized systems under depletion conditions therefore embodies a revision to the general sensitized photoelectrode

design strategies and potentially adds new flexibility in using sensitized photoelectrochemistry for direct solar energy storage in chemical bonds.

■ ASSOCIATED CONTENT

Supporting Information

The Supporting Information contains a detailed description of wxAMPS boundary conditions and simulation parameters, representative capacitance−voltage responses, external quantum yield measurements with and without corrections for solution transmittance for dye concentrations of 5 μM, external quantum yield measurements and solution transmittance measurements for dye concentrations of 50 μM, external quantum yield measurements of three phthalocyanine dyes, absorptance data for the dyes shown in Figure 4, absorptance data for rose bengal tethered to the p-GaP(100) surface and hole injection currents into p-GaP as a function of time throughout the addition of the $O_2(^1\Delta)$ quenchers NaN_3 and histidine. This material is available free of charge via the Internet at http://pubs.acs.org.

■ AUTHOR INFORMATION

Corresponding Author

smald@umich.edu

Author Contributions

[¶]These authors contributed equally to this work

Notes

The authors declare no competing financial interest.

■ ACKNOWLEDGMENTS

The work at the University of Michigan is supported by the U.S. Department of Energy, Basic Energy Sciences under Grant No. DE-SC006628. The work at the University of Illinois is supported by the National Science Foundation under Grant No. CBET-1033615. M.C. acknowledges the support of a DOE Office of Science Graduate Fellowship.

■ REFERENCES

(1) Elliott, C. M. *Nature Chem.* **2011**, *3*, 188−189.
(2) Hardin, B. E.; Snaith, H. J.; McGehee, M. D. *Nat. Photon* **2012**, *6*, 162−169.
(3) Grätzel, M. *Nature* **2001**, *414*, 338−344.
(4) Hamann, T. W.; Jensen, R. A.; Martinson, A. B. F.; Van Ryswyk, H.; Hupp, J. T. *Energy Environ. Sci.* **2008**, *1*, 66−78.
(5) Bandara, J.; Yasomanee, J. P. *Semicond. Sci. Technol.* **2007**, *22*, 20−24.
(6) Borgström, M.; Blart, E.; Boschloo, G.; Mukhtar, E.; Hagfeldt, A.; Hammarström, L.; Odobel, F. *J. Phys. Chem. B* **2005**, *109*, 22928−22934.
(7) Fernando, A. N.; Kitagawa, A.; Suzuki, M.; Takahashi, K.; Komura, T. *Jpn. J. Appl. Phys. 1* **1995**, *34*, 6100−6105.
(8) Gibson, E. A.; Smeigh, A. L.; Le Pleux, L.; Fortage, J.; Boschloo, G.; Blart, E.; Pellegrin, Y.; Odobel, F.; Hagfeldt, A.; Hammarström, L. *Angew. Chem., Int. Ed.* **2009**, *48*, 4402−4405.
(9) He, J. J.; Lindstrom, H.; Hagfeldt, A.; Lindquist, S. E. *J. Phys. Chem. B* **1999**, *103*, 8940−8943.
(10) He, J. J.; Lindstrom, H.; Hagfeldt, A.; Lindquist, S. E. *Sol. Energy Mater.* **2000**, *62*, 265−273.
(11) Li, L.; Gibson, E. A.; Qin, P.; Boschloo, G.; Gorlov, M.; Hagfeldt, A.; Sun, L. C. *Adv. Mater.* **2010**, *22*, 1759−1762.
(12) Morandeira, A.; Boschloo, G.; Hagfeldt, A.; Hammarström, L. *J. Phys. Chem. B* **2005**, *109*, 19403−19410.
(13) Nakasa, A.; Usami, H.; Sumikura, S.; Hasegawa, S.; Koyama, T.; Suzuki, E. *Chem. Lett.* **2005**, *34*, 500−501.
(14) O'Regan, B.; Schwartz, D. T. *Chem. Mater.* **1995**, *7*, 1349−1354.
(15) Qin, P.; Wiberg, J.; Gibson, E. A.; Linder, M.; Li, L.; Brinck, T.; Hagfeldt, A.; Albinsson, B.; Sun, L. C. *J. Phys. Chem. C* **2010**, *114*, 4738−4748.
(16) Sumikura, S.; Mori, S.; Shimizu, S.; Usami, H.; Suzuki, E. *J. Photochem. Photobiol., A* **2008**, *194*, 143−147.
(17) Tennakone, K.; Kahanda, M.; Kasige, C.; Abeysooriya, P.; Wijayanayaka, R. H.; Kaviratna, P. *J. Electrochem. Soc.* **1984**, *131*, 1574−1577.
(18) Zhang, X. L.; Huang, F. Z.; Nattestad, A.; Wang, K.; Fu, D. C.; Mishra, A.; Bauerle, P.; Bach, U.; Cheng, Y. B. *Chem. Commun.* **2011**, *47*, 4808−4810.
(19) Gerischer, H. In *Solar Energy Conversion: Solid-State Physics Aspects*; Seraphin, B. O., Ed.; Springer: Berlin, 1979; Vol. *31*, pp 115−172.
(20) McDaniel, A. M.; Tseng, H. W.; Damrauer, N. H.; Shores, M. P. *Inorg. Chem.* **2010**, *49*, 7981−7991.
(21) Memming, R.; Tributsch, H. *J. Phys. Chem.* **1971**, *75*, 562−570.
(22) Mori, S.; Fukuda, S.; Sumikura, S.; Takeda, Y.; Tamaki, Y.; Suzuki, E.; Abe, T. *J. Phys. Chem. C* **2008**, *112*, 16134−16139.
(23) Fonash, S. J.; Arch, J.; Cuiffi, J.; Hou, J.; Howland, W.; McElheny, P. J.; Moquin, A.; Rogosky, M.; Tran, T.; Zhu, H.; Rubinelli, F. *A Manual for AMPS-1D for Windows 95/NT*; The Pennsylvania State University: Happy Valley, PA, 1997.
(24) McElheny, P. J.; Chatterjie, P.; Fonash, S. J. *J. Appl. Phys.* **1991**, *69*, 7674−7688.
(25) Liu, Y.; Sun, Y.; Rockett, A. *Sol. Energy Mater.* **2012**, *98*, 124−128.
(26) Yuan, Z. L.; Ding, X. M.; Hu, H. T.; Li, Z. S.; Yang, J. S.; Miao, X. Y.; Chen, X. Y.; Cao, X. A.; Hou, X. Y.; Lu, E. D.; Xu, S. H.; Xu, P. S.; Zhang, X. Y. *Appl. Phys. Lett.* **1997**, *71*, 3081−3083.
(27) Price, M. J.; Maldonado, S. *J. Phys. Chem. C* **2009**, *113*, 11988−11994.
(28) Lewis, N. S. *Annu. Rev. Phys. Chem.* **1991**, *42*, 543−580.
(29) Salvador, P. *J. Phys. Chem. B* **2001**, *105*, 6128−6141.
(30) Hagedorn, K.; Forgacs, C.; Collins, S. M.; Maldonado, S. *J. Phys. Chem. C* **2010**, *114*, 12010−12017.
(31) McRae, E. G. *J. Phys. Chem.* **1957**, *61*, 562−572.
(32) Moser, J.; Grätzel, M. *J. Am. Chem. Soc.* **1984**, *106*, 6557−6564.
(33) Lendvay, E. *J. Phys. Chem.* **1965**, *69*, 738−744.
(34) Spitler, M.; Calvin, M. *J. Chem. Phys.* **1977**, *67*, 5193−5200.
(35) Leznoff, C. C.; Lever, A. B. P., Eds. *Phthalocyanines: Properties and Applications*; VCH Publishers: New York, 1993; Vol. *3*.
(36) DeRosa, M. C.; Crutchley, R. J. *Coord. Chem. Rev.* **2002**, *233−234*, 351−371.
(37) Redmond, R. W.; Gamlin, J. N. *Photochem. Photobiol.* **1999**, *70*, 391−475.
(38) Reszka, K.; Cruz, F. S.; Docampo, R. *Chem. Biol. Interact.* **1986**, *58*, 161−172.
(39) Duxbury, D. F. *Chem. Rev.* **1993**, *93*, 381−433.
(40) Spikes, J. D.; Van Lier, J. E.; Bommer, J. C. *J. Photochem. Photobiol. A* **1995**, *91*, 193−198.
(41) Austin, J. M.; Harrison, I. R.; Quickenden, T. I. *J. Phys. Chem.* **1986**, *90*, 1839−1843.
(42) Mori, S.; Fukuda, S.; Sumikura, S.; Takeda, Y.; Tamaki, Y.; Suzuki, E.; Abe, T. *J. Phys. Chem. C* **2008**, *112*, 16134−16139.
(43) Linden, S. M.; Neckers, D. C. *J. Am. Chem. Soc.* **1988**, *110*, 1257−1260.
(44) Adams, R. N.; Galus, Z. *J. Am. Chem. Soc.* **1964**, *86*, 1666−1671.
(45) Grätzel, M.; Frei, H. *J. Phys. Chem.* **1989**, *93*, 7038−7041.
(46) Law, C. H.; Pathirana, S. C.; Li, X.; Anderson, A. Y.; Barnes, P. R. F.; Listorti, A.; Ghaddar, T. H.; O'Regan, B. C. *Adv. Mater.* **2010**, *22*, 4505−4509.
(47) Gershenzon, M.; Mikulyak, R. M. *Appl. Phys. Lett.* **1966**, *8*, 245−247.
(48) Stringfellow, G. B. *J. Vac. Sci. Technol.* **1976**, *13*, 908−913.
(49) Boschloo, G.; Hagfeldt, A. *Acc. Chem. Res.* **2009**, *42*, 1819−1826.
(50) O'Regan, B.; Grätzel, M. *Nature* **1991**, *353*, 737−740.

(51) Yella, A.; Lee, H. W.; Tsao, H. N.; Yi, C. Y.; Chandiran, A. K.; Nazeeruddin, M. K.; Diau, E. W. G.; Yeh, C. Y.; Zakeeruddin, S. M.; Grätzel, M. *Science* **2011**, *334*, 629−634.
(52) Zeng, W.; Cao, Y.; Bai, Y.; Wang, Y.; Shi, Y.; Zhang, M.; Wang, F.; Pan, C.; Wang, P. *Chem. Mater.* **2010**, *22*, 1915−1925.
(53) Planells, M.; Pelleja, L.; Clifford, J. N.; Pastore, M.; De Angelis, F.; Lopez, N.; Marder, S. R.; Palomares, E. *Energy Environ. Sci.* **2011**, *4*, 1820−1829.
(54) Nusbaumer, H.; Zakeeruddin, S. M.; Moser, J. E.; Grätzel, M. *Chem.—Eur. J.* **2003**, *9*, 3756−3763.
(55) Li, R.; Liu, J.; Cai, N.; Zhang, M.; Wang, P. *J. Phys. Chem. B* **2010**, *114*, 4461−4464.
(56) Ghadiri, E.; Taghavinia, N.; Zakeeruddin, S. M.; Grätzel, M.; Moser, J. E. *Nano Lett.* **2010**, *10*, 1632−1638.
(57) Daeneke, T.; Kwon, T. H.; Holmes, A. B.; Duffy, N. W.; Bach, U.; Spiccia, L. *Nature Chem.* **2011**, *3*, 211−215.
(58) Bai, Y.; Yu, Q. J.; Cai, N.; Wang, Y. H.; Zhang, M.; Wang, P. *Chem. Commun.* **2011**, *47*, 4376−4378.
(59) Bessho, T.; Zakeeruddin, S. M.; Yeh, C. Y.; Diau, E. W. G.; Grätzel, M. *Angew. Chem., Int. Ed.* **2010**, *49*, 6646−6649.
(60) Tan, M. X.; Laibinis, P. E.; Nguyen, S. T.; Kesselman, J. M.; Stanton, C. E.; Lewis, N. S. *Prog. Inorg. Chem.* **1994**, *41*, 21−144.
(61) Gibbons, J. F.; Cogan, G. W.; Gronet, C. M.; Lewis, N. S. *Appl. Phys. Lett.* **1984**, *45*, 1095−1097.
(62) Hill, J. J.; Banks, N.; Haller, K.; Orazem, M. E.; Ziegler, K. J. *J. Am. Chem. Soc.* **2011**, *133*, 18663−18672.
(63) Spitler, M. T. *J. Electroanal. Chem.* **1987**, *228*, 69−76.
(64) Parkinson, B. A.; Spitler, M. *Electrochim. Acta* **1992**, *37*, 943−948.
(65) Fillinger, A.; Soltz, D.; Parkinson, B. A. *J. Electrochem. Soc.* **2002**, *149*, A1146−A1156.
(66) Nakao, M.; Itoh, K.; Honda, K. *J. Phys. Chem.* **1984**, *88*, 4906−4907.
(67) Nakao, M.; Itoh, K.; Watanabe, K.; Honda, K. *Ber. Bunsen-Ges. Phys. Chem.* **1985**, *89*, 134−138.
(68) Barnes, P. R. F.; Anderson, A. Y.; Durrant, J. R.; O'Regan, B. C. *Phys. Chem. Chem. Phys.* **2011**, *13*, 5798−5816.
(69) Gonzalez-Vazquez, J. P.; Anta, J. A.; Bisquert, J. *J. Phys. Chem. C* **2010**, *114*, 8552−8558.
(70) Han, L. Y.; Koide, N.; Chiba, Y.; Mitate, T. *Appl. Phys. Lett.* **2004**, *84*, 2433−2435.
(71) Han, L. Y.; Koide, N.; Chiba, Y.; Islam, A.; Mitate, T. *C. R. Chim.* **2006**, *9*, 645−651.
(72) Lee, J. J.; Coia, G. M.; Lewis, N. S. *J. Phys. Chem. B* **2004**, *108*, 5282−5293.
(73) Murayama, M.; Mori, T. *Thin Solid Films* **2006**, *509*, 123−126.
(74) Penny, M.; Farrell, T.; Please, C. *Sol. Energy Mater.* **2008**, *92*, 11−23.
(75) Penny, M.; Farrell, T.; Will, G. *Sol. Energy Mater.* **2008**, *92*, 24−37.
(76) Södergren, S.; Hagfeldt, A.; Olsson, J.; Lindquist, S. E. *J. Phys. Chem.* **1994**, *98*, 5552−5556.
(77) Royea, W. J.; Kruger, O.; Lewis, N. S. *J. Electroanal. Chem.* **1997**, *438*, 191−197.
(78) Foley, J. M.; Price, M. J.; Feldblyum, J. I.; Maldonado, S. *Energy Environ. Sci.* **2012**, *5*, 5203−5220.
(79) Law, M.; Greene, L. E.; Johnson, J. C.; Saykally, R.; Yang, P. D. *Nat. Mater.* **2005**, *4*, 455−459.
(80) Baxter, J. B.; Aydil, E. S. *Appl. Phys. Lett.* **2005**, 86.
(81) Tan, B.; Wu, Y. Y. *J. Phys. Chem. B* **2006**, *110*, 15932−15938.
(82) Wen, W.; Carim, A. I.; Collins, S. M.; Price, M. J.; Peczonczyk, S. L.; Maldonado, S. *J. Phys. Chem. C* **2011**, *115*, 22652−22661.
(83) Schuurmans, F. J. P.; Megens, M.; Vanmaekelbergh, D.; Lagendijk, A. *Phys. Rev. Lett.* **1999**, *83*, 2183−2186.
(84) Khaselev, O.; Turner, J. A. *J. Electrochem. Soc.* **1998**, *145*, 3335−3339.
(85) Lewerenz, H. J.; Aspnes, D. E.; Miller, B.; Malm, D. L.; Heller, A. *J. Am. Chem. Soc.* **1981**, *104*, 3325−3329.
(86) Mukherjee, J.; Peczonczyk, S.; Maldonado, S. *Langmuir* **2010**, *26*, 10890−10896.
(87) Peczonczyk, S. L.; Mukherjee, J.; Carim, A. I.; Maldonado, S. *Langmuir* **2012**, *28*, 4672−4682.
(88) Heller, A.; Miller, B.; Thiel, F. A. *Appl. Phys. Lett.* **1981**, *38*, 282−284.
(89) Aharon-Shalom, E.; Heller, A. *J. Electrochem. Soc.* **1982**, *129*, 2865−2866.
(90) Berger, L. I. *Semiconductor Materials*; CRC Press, Inc.: Boca Raton, 1997.
(91) Schroten, E.; Goossens, A.; Schoonman, J. *J. Appl. Phys.* **1996**, *79*, 4465−4467.
(92) Collins, S. M.; Hankett, J. M.; Carim, A. I.; Maldonado, S. *J. Mater. Chem.* **2012**, *22*, 6613−6622.
(93) McCormick, T. M.; Calitree, B. D.; Orchard, A.; Kraut, N. D.; Bright, F. V.; Detty, M. R.; Eisenberg, R. *J. Am. Chem. Soc.* **2010**, *132*, 15480−15483.